Journal of Computational Mathematics
Vol.xx, No.x, 2025, 1–18.

http://www.global-sci.org/jcm
doi:10.4208/jcm.2505-m2025-0028

GEOMETRIC PROPERTIES AND ALGORITHMS OF THE HYBRID PATCH WITH B-SPLINE BOUNDARIES*

Ying-Chun Wang and Chun-Gang Zhu[1)]
School of Mathematical Sciences, Dalian University of Technology, Dalian 116024, China;
Key Laboratory for Computational Mathematics and Data Intelligence of Liaoning Province, Dalian 116024, China
Emails: wangyc992@mail.dlut.edu.cn, cgzhu@dlut.edu.cn

Abstract

The hybrid patch proposed by Salvi effectively integrates both ribbon-based and control-based surfaces, thereby inheriting the advantages of each. This new multi-sided patch representation represents an improvement over Kato's patch by incorporating interior control. It is also more versatile than the generalized Bézier surfaces, as it can handle positional and cross-derivative boundary constraints of arbitrary degrees. In this paper, we study the geometric properties and algorithms of the hybrid patch with B-spline boundaries. We first demonstrate that the hybrid patch possesses boundary interpolation and boundary derivative interpolation. The original degree elevation by Salvi changes the geometry of the patch slightly, which makes it undesirable in some applications. To address this issue, we propose an improved degree elevation algorithm for the hybrid patch, which preserves the geometric consistency of the patch. Furthermore, based on the knot insertion algorithm for B-splines, we propose a novel knot insertion algorithm for the hybrid patch with B-spline boundaries. Some representative examples show the effectiveness and validity of the proposed results.

Mathematics subject classification: 65D07, 65D17, 68U07.
Key words: Hybrid patch, B-splines, Boundary property, Degree elevation, Knot insertion.

1. Introduction

The representation of parametric surfaces is one of the core fields in computer aided geometric design (CAGD) [4] and computer aided design (CAD), which has made great progress over the past few decades with the rapid development of computers. Parametric surface modeling plays a crucial role in various practical applications, especially in automotive, aerospace, and architecture. In terms of geometric modeling, several powerful tools have been developed, including Bézier method, B-spline method, and industry-standard non-uniform rational B-spline (NURBS) method [16].

The B-spline method, which employs the standard B-spline basis functions and control points for curve, surface, or volume construction, addresses the limitations of the Bézier method and serves as a generalization of the Bézier method, proving to be more versatile in practical applications. Nowadays, the B-spline method has become a significant tool in geometric modeling in the world. However, in practical applications, existing tools often fall short in representing

* Received January 21, 2025 / Revised version received April 2, 2025 / Accepted May 12, 2025 / Published online November 12, 2025 /
1) Corresponding author

the n-sided ($n > 4$) surfaces, which are necessary for complex domain representation. As a result, multi-sided patches, including S-patches [14], toric surfaces [12], and generalized Bézier (GB) surfaces [25], have garnered extensive research attention [6, 22, 26, 33]. For the traditional surface design, the control point-based surface representation has some advantages in research and applications. Although toric surfaces and GB surfaces are control point-based representations, they are limited to constructing surfaces with Bézier boundaries and cannot generalize to B-spline boundaries.

Hughes *et al.* [9] and Cottrell *et al.* [2] proposed the concept of isogeometric analysis (IGA), which aims to bridge the gap between finite element analysis (FEA) and CAD. Given the boundary representation of a CAD model, constructing a analysis-suitable parameterization of computational domain is a crucial task in IGA and the quality of parameterization dramatically affects the accuracy and efficiency of the subsequent analysis [31]. The degree elevation and knot insertion algorithms are two of the most crucial techniques in the B-spline method. By degree elevation and knot insertion, the number of control points can be increased, which enhances the degrees of freedom (DOFs). These enhancements are vital for IGA because it allows for improvement of PDE solving accuracy over complex CAD geometry, called p-refinement (degree elevation), h-refinement (knot insertion) and k-refinement (both). Li *et al.* [13] proposed a de Casteljau algorithm and a degree elevation algorithm for toric surfaces and applied the degree elevation algorithm of toric surfaces to IGA. Ji *et al.* [10] proposed a novel h-refinement scheme in IGA with planar multi-sided toric surface patches. Wang *et al.* [30] proposed an improved degree elevation algorithm for GB surfaces and a new GB surface knot insertion algorithm based on the properties of the basis function, employing these algorithms to refine the GB parameterizations of computational domains in IGA. There are also many literatures discussing the application of geometric algorithms in IGA [7, 12, 32]. How to construct analysis-suitable parameterizations of multi-sided complex computational domains with B-spline boundaries and then provide efficient refinement strategies to increase the accuracy in analysis are challenging problems in IGA.

Recently, Salvi [18] introduced a new multi-sided parametric patch construction scheme, known as the hybrid patch, which integrates the benefits of ribbon-based [20, 24, 27] and control-point-based [19, 23, 29] methods. The hybrid patch can handle position and cross-derivative boundary constraints of any degree while also allowing for control over the interior of the surface. Although the hybrid patch has good properties, the degree elevation algorithm introduced in [18] may change the geometrical shape of the original surface, making it unsuitable for some applications, especially for IGA [3]. Recently, Várady *et al.* [28] proposed a new scheme for GB/GBS surfaces that preserves the interior of the surface algebraically while refining the boundary ribbons by degree elevation/knot insertion.

In this paper, our study focuses on the hybrid patch with B-spline boundaries, since the boundaries of CAD models are generally presented by B-splines. We explore the geometric properties of the hybrid patch with B-spline boundaries, including the boundary interpolation property and the boundary derivative interpolation property. The research of surface blending and the filling of multi-sided surface holes holds significant practical value and has garnered considerable attention from many scholars [8, 11, 15, 17, 21]. We also propose an improved degree elevation algorithm for the hybrid patch with B-spline boundaries and a novel knot insertion algorithm to enable local control for the hybrid patch. These two algorithms both keep the patch interior and boundary unchanged and provide the application to the refinements in IGA. Several examples are given to demonstrate the effectiveness and validity of the proposed algorithms.

The rest of this paper is structured as follows. In Section 2, we review the definitions of B-splines and the hybrid patch. In Section 3, the properties of boundary interpolation and boundary derivative interpolation of the hybrid patch are presented. In Section 4, we propose an improved degree elevation algorithm and a novel knot insertion algorithm for the hybrid patch. And some examples are given to show the effectiveness and validity of the proposed results. Finally, the paper concludes with a summary and future work in Section 5.

2. Preliminaries

In this section, we briefly introduce the definition of the B-spline basis functions, and the degree elevation and knot insertion algorithms of the B-splines. And then we review the definition of the hybrid patch proposed in [18].

2.1. B-splines

The B-spline basis functions, as piecewise polynomials, not only inherit the advantages of simplicity and computational convenience form of polynomials but also possess the property of local control. B-spline curves and surfaces can be structured using standard B-spline basis functions. The B-spline curve constructed by the B-spline basis functions retains the advantages of the Bézier curve and is a generalization of the Bézier curve.

Definition 2.1 (B-spline Basis Function). *For a given knot vector* $\mathbf{U}=\{t_0, t_1, \cdots, t_{n+p+1}\}$*, its knots satisfy* $t_j \leq t_{j+1}$*. The B-spline basis functions of degree* p *defined on the knot vector* $\mathbf{U}$ *can be computed recursively using the following de Boor-Cox formula:*

$$\begin{cases} N_i^{0,\mathbf{U}}(t) = \begin{cases} 1, & t \in [t_j, t_{j+1}), \\ 0, & otherwise, \end{cases} \\ N_i^{p,\mathbf{U}}(t) = \dfrac{t - t_i}{t_{i+p} - t_i} N_i^{p-1,\mathbf{U}}(t) + \dfrac{t_{i+p+1} - t}{t_{i+p+1} - t_{i+1}} N_{i+1}^{p-1,\mathbf{U}}(t), \quad p \geq 1, \end{cases}$$

therein stipulate $0/0 = 0$*.*

Definition 2.2 (B-spline Curve). *The B-spline curve of degree* p *is defined as*

$$\mathbf{P}(t) = \sum_{i=0}^{n} \mathbf{P}_i N_i^{p,\mathbf{U}}(t), \quad t \in [t_p, t_{n+1}],$$

where $N_i^{p,\mathbf{U}}(t), i = 0, 1, \ldots, n$*, are the B-spline basis functions of degree* p *defined on the knot vector* $\mathbf{U} = \{t_0, t_1, \cdots, t_{n+p+1}\}$*. The points* $\mathbf{P}_i \in \mathbb{R}^3, i = 0, 1, \ldots, n$*, are called the control points.*

The B-spline surfaces are defined by the tensor-product B-spline basis functions in the same way and we will omit the details here. The degree elevation and the knot insertion algorithms for B-splines are important geometric algorithms. The degree elevation algorithm enhances the flexibility of curve shape control. The number of control points of the B-splines can be added by elevating the degrees, which increases the DOFs. Additionally, inserting knots improves the locality of B-splines. In fact, the B-splines remain unchanged after degree elevation and knot insertion. We can find the detailed formula for the geometric algorithms of B-splines in [16].

2.2. Hybrid patch

The hybrid patch can handle positional and cross-derivative boundary constraints of any degree while providing intuitive control over the patch interior. It is a rational polygonal patch defined over n-sided convex domain Γ (see Fig. 2.1(a) for an example). The definition of the hybrid patch needs local parameters $s_i = s_i(u,v)$ and $h_i = h_i(u,v)$ which are computed by Wachspress barycentric coordinates λ_i. We introduce the expression of Wachspress coordinates [5] as follow.

Definition 2.3 ([5]). *For a given n-sided convex polygonal domain Γ with its vertices $\mathbf{v}_1, \cdots, \mathbf{v}_n$ $(n \geq 4)$, denote its outward unit normal to the edge $\mathbf{e}_i = \overline{\mathbf{v}_{i-1}\mathbf{v}_i}$ by $\mathbf{n}_i = (n_1^i, n_2^i)^\top$. Let $\phi_i^\perp(\mathbf{x})$ be the perpendicular distance of $\mathbf{x}$ to the edge $\mathbf{e}_i$, that is,*

$$\phi_i^\perp(\mathbf{x}) = (\mathbf{v}_i - \mathbf{x}) \cdot \mathbf{n}_i, \quad \forall\, \mathbf{x} \in \Gamma. \tag{2.1}$$

Then, the Wachspress barycentric coordinates is defined as

$$\lambda_i(\mathbf{x}) = \frac{w_i(\mathbf{x})}{\sum_{j=1}^n w_j(\mathbf{x})}, \quad i = 1, \ldots, n, \tag{2.2}$$

where

$$w_i(\mathbf{x}) := \frac{\langle \mathbf{n}_{i-1}, \mathbf{n}_i \rangle}{\phi_{i-1}^\perp(\mathbf{x})\phi_i^\perp(\mathbf{x})}, \tag{2.3}$$

and $\langle \mathbf{n}_{i-1}, \mathbf{n}_i \rangle = n_1^{i-1} n_2^i - n_2^{i-1} n_1^i$.

With Wachspress barycentric coordinates in hand, the hybrid patch can be defined directly.

Definition 2.4 ([18]). *Given an n-sided convex polygonal domain Γ, denote the Wachspress barycentric coordinates of Γ by $\lambda_i, i = 1, \ldots, n$. Given the control points $\mathbf{C}_{j,k}^{d,i}, j = 0, \ldots, d$, $k = 0, \ldots, l-1$, where d is the degree of the Bernstein basis functions, $l = \lceil d/2 \rceil$ is the number of control point layers. The control points around the corners are shared by the two adjacent patches, i.e.*

$$\mathbf{C}_{p,q}^{d,i} = \mathbf{C}_{d-q,p}^{d,i-1}, \quad p, q = 0, \ldots, l-1.$$

The hybrid patch is the image of the mapping $\mathbf{S} : \Gamma \to \mathbb{R}^3$, for any $(u,v) \in \Gamma$,

$$\mathbf{S}(u,v) = \sum_{i=1}^{n} \left[\sum_{j=0}^{d} \sum_{k=2}^{l-1} \mathbf{C}_{j,k}^{d,i} \mu_{j,k}^i B_{j,k}^{d,d}\big(s_i(u,v), h_i(u,v)\big) + \mathbf{R}_i(s_i, h_i) L_i^*(u,v) \right] + \mathbf{C}_0^d B_0^d(u,v), \tag{2.4}$$

where

$$s_i = \frac{\lambda_i}{\lambda_{i-1} + \lambda_i}, \quad h_i = 1 - \lambda_{i-1} - \lambda_i \tag{2.5}$$

are the local side and distance parameters,

$$B_{j,k}^{d,d}(s_i, h_i) = B_j^d(s_i) B_k^d(h_i) = \binom{d}{j} (1-s_i)^{d-j} s_i^j \binom{d}{k} (1-h_i)^{d-k} h_i^k$$

are Bernstein basis functions of (s_i, h_i), the ribbon $\mathbf{R}_i(s_i, h_i)$ is a quadrilateral surface interpolating the i-th boundary curve,

$$L_i^*(u,v) = \sum_{j=0}^{d} \sum_{k=0}^{1} \mu_{j,k}^i(h_1, \ldots, h_n) B_{j,k}^{d,d}(s_i, h_i) \tag{2.6}$$

are the weight sum of the two rows,

$$\mathbf{C}_0^d = \frac{1}{n}\sum_{i=1}^{n}\mathbf{C}_{l,l-1}^{d,i} \tag{2.7}$$

is the central point, and its corresponding blending function

$$B_0^d(u,v) = 1 - B_\Sigma(u,v) = 1 - \sum_{i=1}^{n}\sum_{j=0}^{d}\sum_{k=0}^{l-1}\mu_{j,k}^{i}B_{j,k}^{d,d}\big(s_i(u,v), h_i(u,v)\big), \tag{2.8}$$

the weights

$$\mu_{j,k\,j\le d/2}^{i} = \begin{cases} 0, & j<k, \quad k\ge 2,\\ \dfrac{1}{2}, & 2\le j=k<l,\\ \alpha_i = \dfrac{h_{i-1}^2}{h_{i-1}^2+h_i^2}, & j,k<2,\\ 1, & \textit{otherwise}, \end{cases}$$

$$\mu_{j,k\,j> d/2}^{i} = \begin{cases} 0, & j>d-k, \quad k\ge 2,\\ \dfrac{1}{2}, & j=d-k, \quad k\ge 2,\\ \beta_i = \dfrac{h_{i+1}^2}{h_{i+1}^2+h_i^2}, & j>d-2, \quad k<2,\\ 1, & \textit{otherwise}. \end{cases}$$

Remark 2.1. The definition of s_i in Definition 2.4 is undefined for points on the distant sides $\mathbf{e}_i, i\notin\{i-1,i,i+1\}$. This results in the basis functions and the hybrid patch being discontinuous along the boundary. To circumvent this problem, we use the equivalent definition of s_i proposed in [25]

$$s_i = \frac{\sin(\theta_i)\phi_{i-1}^{\perp}}{\sin(\theta_i)\phi_{i-1}^{\perp}+\sin(\theta_{i-1})\phi_{i+1}^{\perp}}, \tag{2.9}$$

where θ_i is the angle at $\mathbf{v}_i$. The resulting basis functions remain continuous across the entire parametric domain Γ, which is advantageous for subsequent analysis and computations.

Remark 2.2. The i-th ribbon $\mathbf{R}_i(s_i,h_i)$ in (2.4) can be defined as

$$\mathbf{R}_i(s_i,h_i) = \mathbf{P}_i(s_i) + h_i\mathbf{T}_i(s_i), \tag{2.10}$$

the $\mathbf{P}_i(s_i)$ is the boundary curve along the i-th side and the $\mathbf{T}_i(s_i)$ is the cross-tangent function associated with the boundary [27]. We define the $\mathbf{P}_i(s_i)$ and $\mathbf{T}_i(s_i)$ of the ribbon $\mathbf{R}_i$ in the forms of

$$\begin{aligned} \mathbf{P}_i(s_i) &= \sum_{j=0}^{d}\mathbf{C}_{j,0}^{d,i}N_j^{p_i,\mathbf{U}_i^b}(s_i),\\ \mathbf{T}_i(s_i) &= \sum_{j=0}^{d}\frac{p_i}{\mathbf{U}_{i,p+j}^b-\mathbf{U}_{i,j}^b}\big(\mathbf{C}_{j,1}^{d,i}-\mathbf{C}_{j,0}^{d,i}\big)N_j^{p_i,\mathbf{U}_i^b}(s_i), \end{aligned} \tag{2.11}$$

where the B-spline basis functions $N_j^{p_i,\mathbf{U}_i^b}(s_i)$ at side i have degree p_i and knot vector $\mathbf{U}_i^b$. Therefore, the hybrid patch $\mathbf{S}(u,v)$ in (2.4) can be expressed as $\mathbf{S}^{d,\mathbf{p}}(u,v)(\mathbf{p}=\{p_1,\cdots,p_n\})$.

If the degrees and knot vectors of the B-splines are the same on each side,that is, the $\mathbf{P}_i(s_i)$ and $\mathbf{T}_i(s_i)$ defined in the forms of

$$\begin{aligned}\mathbf{P}_i(s_i) &= \sum_{j=0}^{d} \mathbf{C}_{j,0}^{d,i} N_j^{p,\mathbf{U}^b}(s_i),\\ \mathbf{T}_i(s_i) &= \sum_{j=0}^{d} \frac{p}{\mathbf{U}_{p+j}^b - \mathbf{U}_j^b}\left(\mathbf{C}_{j,1}^{d,i} - \mathbf{C}_{j,0}^{d,i}\right) N_j^{p,\mathbf{U}^b}(s_i),\end{aligned} \tag{2.12}$$

the hybrid patch $\mathbf{S}(u,v)$ in (2.4) can be expressed as $\mathbf{S}^{d,p}(u,v)$.

The hybrid patch representation is a generalization of the GB surfaces because it adds interior control and is not limited to polynomial boundaries. In this paper, we focus on the hybrid patch with B-spline boundaries, so we explain how to construct a hybrid patch from given B-spline boundaries through the following example. More details about the hybrid patch are available in [18] and references therein.

Example 2.1. Given $d = 6, l = 3, n = 5$. Consider a pentagonal parametric domain

$$\Gamma = \mathrm{Conv}\left\{(0,0),(1,0),\left(1,\frac{1}{2}\right),\left(\frac{1}{2},1\right),(0,1)\right\}$$

as shown in Fig. 2.1(a). The $\mathbf{P}_i(s_i)$ and $\mathbf{T}_i(s_i)$ of the ribbon $\mathbf{R}_i$ are defined in (2.12), where the degree and knot vector of the B-spline basis functions $N_j^{p,\mathbf{U}^b}(s_i)$ are $p = 2$ and

$$\mathbf{U}^b = \{0,0,0,0.2,0.4,0.6,0.8,1,1,1\}.$$

Fig. 2.1(b) shows the corresponding pentagonal hybrid patch $\mathbf{S}^{6,2}$.

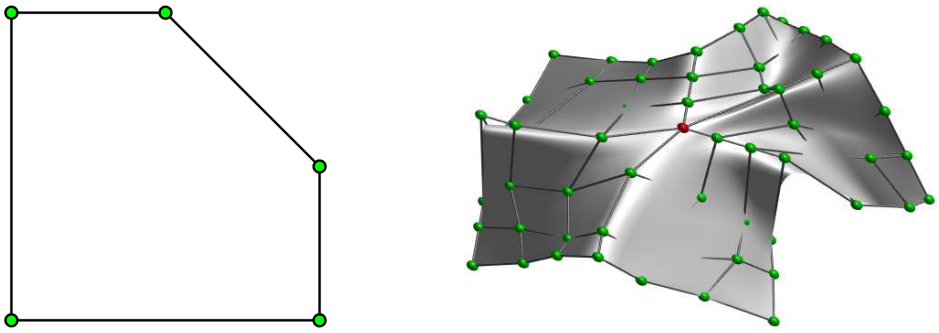

(a) Pentagonal parametric domain (b) Pentagonal hybrid patch

Fig. 2.1. Pentagonal parametric domain and hybrid patch.

3. Boundary Properties of the Hybrid Patch

In this section, we will demonstrate both the boundary interpolation property and boundary derivative interpolation property of the hybrid patch, along with the corresponding proofs.

3.1. Boundary interpolation

We define a side interpolant $\mathbf{I}_i(s_i, h_i)$ as B-spline surfaces of bi-degree $p_i \times p_i$, created by the first two layers of control points for each sides

$$\mathbf{I}_i(s_i, h_i) = \sum_{j=0}^{d} \sum_{k=0}^{1} \mathbf{C}_{j,k}^{d,i} N_j^{p_i, \mathbf{U}_i^b}(s_i) N_k^{p_i, \mathbf{U}_i^b}(h_i).$$

Then, we conclude the following boundary interpolation property.

Theorem 3.1. *Given a n-sided convex polygonal domain Γ, the hybrid patch is defined as* (2.4)*. The hybrid patch interpolates the B-spline boundaries, that is, when the local distance parameter $h_i = 0$ on the side Γ_i for all points (u, v) on the i-th side, we have*

$$\mathbf{S}^{d,\mathbf{P}}(u, v) = \mathbf{P}_i(s_i) = \mathbf{I}_i(s_i, 0).$$

Proof. The "contribution" of the i-th side can be written as

$$\mathbf{S}_i(s_i, h_i) = \sum_{j=0}^{d} \sum_{k=2}^{l-1} \mathbf{C}_{j,k}^{d,i} \mu_{j,k}^i B_{j,k}^{d,d}(s_i, h_i) + \mathbf{R}_i(s_i, h_i) L_i^*(u, v), \tag{3.1}$$

then the hybrid patch can be represented as

$$\mathbf{S}^{d,\mathbf{P}}(u, v) = \sum_{i=1}^{n} \mathbf{S}_i(s_i, h_i) + \mathbf{C}_0^d B_0^d(u, v). \tag{3.2}$$

(i) $\mathbf{S}_i(s_i, h_i)$ does not affect the distant sides $\Gamma_j, j \notin \{i-1, i, i+1\}$, in positional sense. Because the h_i equals 1 on the distant sides Γ_j by definition. We obtain

$$B_k^d(h_i) = B_k^d(1) = 0, \quad k \in \{0, \ldots, l-1\},$$

by the endpoint property of the Bernstein basis function

$$B_k^d(1) = \begin{cases} 1, & k = d, \\ 0, & k \neq d. \end{cases}$$

The Bernstein functions vanish, so we have $\mathbf{S}_i(s_i, h_i) = \mathbf{0}$.

(ii) $\mathbf{S}_i(s_i, h_i)$ does not affect the adjacent sides Γ_{i-1} and Γ_{i+1} in positional sense. Because $s_i = 0$ on the side Γ_{i-1} and $h_{i-1} = s_i = 0$. So we obtain

$$B_j^d(s_i) = B_j^d(0) = 0, \quad j \in \{1, \ldots, d\}.$$

The $\mathbf{S}_i(s_i, h_i)$ in (3.1) can be represented as

$$\mathbf{S}_i(s_i, h_i) = \sum_{k=2}^{l-1} \mathbf{C}_{0,k}^{d,i} \mu_{0,k}^i B_k^d(h_i) + \mathbf{R}_i(s_i, h_i) \sum_{k=0}^{1} \mu_{0,k}^i B_k^d(h_i).$$

For $k \geq 2$, the multiplier $\mu_{0,k}^i = 0$ by definition, and for $k < 2$, the multiplier

$$\mu_{0,k}^i = \alpha_i = \frac{h_{i-1}^2}{h_{i-1}^2 + h_i^2} = 0,$$

due to $h_{i-1} = 0$. The weighted Bernstein functions vanish, so we have $\mathbf{S}_i(s_i, h_i) = \mathbf{0}$. For Γ_{i+1} we proceed in the same way.

(iii) $\mathbf{S}_i(s_i, h_i)$ reproduces the related boundary curve $\mathbf{P}_i(s_i)$ on Γ_i. Because when $h_i = 0$, we obtain $B_k^d(h_i) = B_k^d(0) = 0, k \in \{1, \ldots, l-1\}$, by the endpoint property of the Bernstein basis functions

$$B_k^d(0) = \begin{cases} 1, & k = 0, \\ 0, & k \neq 0. \end{cases}$$

The $\mathbf{S}_i(s_i, h_i)$ in (3.1) can be represented as

$$\mathbf{S}_i(s_i, h_i) = \mathbf{P}_i(s_i) \sum_{j=0}^{d} \mu_{j,0}^i B_j^d(s_i).$$

For $0 \leq j \leq d$, all $\mu_{j,0}^i$ are equal to 1, since $h_i = 0$. Then we have $\mathbf{S}_i(s_i, h_i) = \mathbf{P}_i(s_i)$ by the partition of unity of the Bernstein basis functions.

To sum up, we have shown that the boundaries of the hybrid patch are the curves defined by $\mathbf{P}_i(s_i), i = 1, \ldots, n$ exactly. □

To validate the correctness of the property presented in Theorem 3.1, we present an example showing that the boundaries of the hybrid patch defined by (2.11) are the boundary B-spline curves exactly.

Example 3.1. Given $d = 6, l = 3, n = 6$. Consider a hexagonal parametric domain

$$\Gamma = \text{Conv}\left\{\left(\frac{1}{3}, 0\right), (1, 0), \left(1, \frac{2}{3}\right), \left(\frac{2}{3}, 1\right), (0, 1), \left(0, \frac{1}{3}\right)\right\}.$$

The $\mathbf{P}_i(s_i)$ and $\mathbf{T}_i(s_i)$ of ribbon $\mathbf{R}_i$ are defined in (2.11). Given the degrees of boundaries as $p_1 = 5, p_2 = 3, p_3 = 2, p_4 = 4, p_5 = 4, p_6 = 2$ and their knot vectors

$$\begin{aligned}
\mathbf{U}_1^b &= \{0, 0, 0, 0, 0, 0, 0.5, 1, 1, 1, 1, 1, 1\}, \\
\mathbf{U}_2^b &= \{0, 0, 0, 0, 0.2, 0.5, 0.8, 1, 1, 1, 1\}, \\
\mathbf{U}_3^b &= \{0, 0, 0, 0.1, 0.3, 0.7, 0.9, 1, 1, 1\}, \\
\mathbf{U}_4^b &= \{0, 0, 0, 0, 0, 0.4, 0.8, 1, 1, 1, 1, 1\}, \\
\mathbf{U}_5^b &= \{0, 0, 0, 0, 0, 0.3, 0.7, 1, 1, 1, 1, 1\}, \\
\mathbf{U}_6^b &= \{0, 0, 0, 0.2, 0.4, 0.6, 0.8, 1, 1, 1\}.
\end{aligned}$$

Fig. 3.1(a) shows the corresponding hexagonal hybrid patch interpolating these six B-spline boundaries which are generated by boundary control points and corresponding B-spline basis functions. In the same way, given $d = 6, l = 3, n = 8$, consider a octagonal parametric domain

$$\Gamma = \text{Conv}\left\{\left(\frac{1}{4}, 0\right), \left(\frac{3}{4}, 0\right), \left(1, \frac{1}{4}\right), \left(1, \frac{3}{4}\right), \left(\frac{3}{4}, 1\right), \left(\frac{1}{4}, 1\right), \left(0, \frac{3}{4}\right), \left(0, \frac{1}{4}\right)\right\}.$$

We show the octagonal hybrid patch interpolating eight B-spline boundaries in Fig. 3.1(b).

From our findings, we conclude that the hybrid patch defined by (2.11) interpolates B-spline boundaries. That means we can construct the hybrid patch from given B-spline boundaries of any degree and knot vector. This result is useful for constructing domain parameterization of CAD model with complex multi-sided boundary representation, which is a key step in IGA.

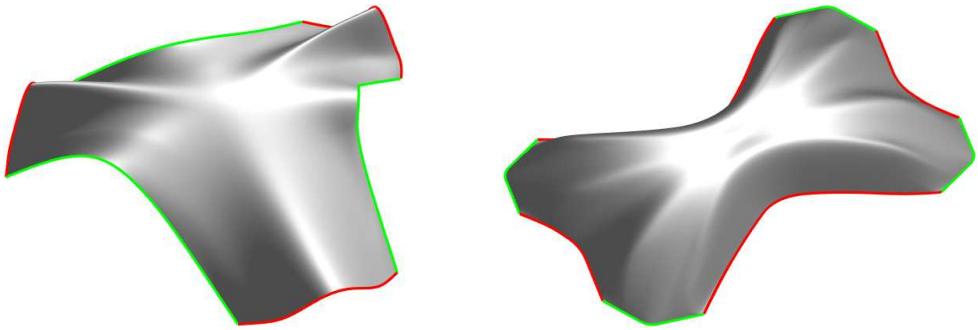

(a) Hexagonal hybrid patch (b) Octagonal hybrid patch

Fig. 3.1. Boundary interpolation property of hybrid patches.

3.2. Boundary derivative interpolation

To demonstrate that the hybrid patch with B-spline boundaries satisfies derivative interpolation conditions along the boundaries, we establish the following result. Our proof uses the recursive formula of Bernstein derivative function, that is

$$\begin{aligned}\left[B_k^d(h_i)\right]' &= d\left[B_{k-1}^{d-1}(h_i) - B_k^{d-1}(h_i)\right] \\ &= \frac{d!}{(k-1)!(d-k)!}h_i^{k-1}(1-h_i)^{d-k} \\ &\quad - \frac{d!}{k!(d-k-1)!}h_i^k(1-h_i)^{d-k-1},\end{aligned}$$

where

$$B_{-1}^{d-1}(h_i) = B_d^{d-1}(h_i) = 0.$$

Theorem 3.2. *Given a n-sided convex polygonal domain Γ, the hybrid patch is defined as (2.4). The hybrid patch interpolate the cross-tangent of the respective sides, that is, when the local distance parameter $h_i = 0$ on the side Γ_i, for all points (u, v) on the i-th side, we have*

$$\left(\mathbf{S}^{d,\mathbf{P}}(u,v)\right)' = \mathbf{T}_i(s_i),$$

where $\left(\mathbf{S}^{d,\mathbf{P}}(u,v)\right)'$ denotes a derivative of h_i.

Proof. First, we investigate the derivatives of weighted Bernstein functions $[\mu_{j,k}^i B_{j,k}^{d,d}(s_i,h_i)]'$, when $j \in \{0,\ldots,d\}$ and $k \in \{2,\ldots,l-1\}$.

According to the definition of weights $\mu_{j,k}^i$, it is constant when $k \geq 2$. So, it is equal to investigate the derivatives $\mu_{j,k}^i B_j^d(s_i)[B_k^d(h_i)]'$. From the recursive formula of Bernstein derivative function, we obtain that the derivative of $[B_k^d(h_i)]', k \in \{2,\ldots,l-1\}$ have the term h_i since $k \geq 2$ and $d - l > 0$. For side Γ_i ($h_i = 0$), the derivatives of the weighted Bernstein functions vanish. For other sides $\Gamma_m, m \notin \{i\}$, the derivatives $\mu_{j,k}^m B_j^d(s_m)[B_k^d(h_m)]'$ do not have the term h_i, therefore,the derivatives vanish. Then, we obtain that the equation

$$\sum_{i=1}^{n}\sum_{j=0}^{d}\sum_{k=2}^{l-1}\mathbf{C}_{j,k}^{d,i}\left[\mu_{j,k}^i B_{j,k}^{d,d}(s_i,h_i)\right]' = \mathbf{0}. \tag{3.3}$$

Next, we investigate the derivatives $[\mathbf{R}_i(s_i,h_i)L_i^*(s_i,h_i)]'$. Our proof consists of three parts.

(i) For the distant sides $\Gamma_m, m \notin \{i-1, i, i+1\}$, due to $h_m = 1$ on side Γ_i, $B_k^d(h_m) = 0$ and $[B_k^d(h_m)]' = 0$ when $j \in \{0, \ldots, d\}$ and $k \in \{0, 1\}$. We also have $L_i^*(s_m, h_m) = 0$. Therefore, the derivatives $[\mathbf{R}_m(s_m, h_m)L_m^*(s_m, h_m)]' = \mathbf{0}, m \notin \{i-1, i, i+1\}$.

(ii) Next look at the derivative of $\mathbf{R}_{i-1}(s_{i-1}, h_{i-1})L_{i-1}^*(s_{i-1}, h_{i-1})$ on the side Γ_i. According to the definition of weights $\mu_{j,k}^{i-1}$ $(k < 2)$, only when $j \in \{d-1, d\}, \beta_{i-1}$ have the term h_i. Due to $s_{i-1} = 1$ on the side Γ_i, we can obtain

$$[\mathbf{R}_{i-1}L_{i-1}^*]' = \mathbf{R}_{i-1}(s_{i-1}, h_{i-1})[\beta_{i-1}]' \sum_{k=0}^{1} B_k^d(h_{i-1}).$$

In the same way, according to the definition of weights $\mu_{j,k}^{i+1}$ $(k < 2)$, only when $j \in \{0, 1\}, \alpha_{i+1}$ have the term h_i. Due to $s_{i+1} = 0$ on the side Γ_i, we can obtain

$$[\mathbf{R}_{i+1}L_{i+1}^*]' = \mathbf{R}_{i+1}(s_{i+1}, h_{i+1})[\alpha_{i+1}]' \sum_{k=0}^{1} B_k^d(h_{i+1}).$$

Since $h_i = 0$ on the side Γ_i, we have

$$[\beta_{i-1}]' = \left[\frac{h_i^2}{h_i^2 + h_{i-1}^2}\right]' = 0, \quad [\alpha_{i+1}]' = \left[\frac{h_i^2}{h_i^2 + h_{i+1}^2}\right]' = 0.$$

Then, we can obtain the derivatives $[\mathbf{R}_{i-1}L_{i-1}^*]' = \mathbf{0}$ and $[\mathbf{R}_{i+1}L_{i+1}^*]' = \mathbf{0}$.

(iii) In the end, we show the reproduction of the cross-derivative function $\mathbf{T}_i(s_i)$ on Γ_i. Since $h_i = 0, L_i^*(s_i, h_i) = 1$ and the definition of the weights $\mu_{j,k}^i$, we have

$$[\mathbf{R}_i(s_i, h_i)L_i^*(s_i, h_i)]' = \mathbf{R}_i'(s_i, h_i) + \mathbf{R}_i(s_i, h_i)\left(\sum_{j=0}^{1}[\alpha_i]' B_j^d(s_i) + \sum_{j=d-1}^{d}[\beta_i]' B_j^d(s_i)\right).$$

Since $h_i = 0$ on the side Γ_i, we have

$$[\alpha_i]' = \left[\frac{h_{i-1}^2}{h_{i-1}^2 + h_i^2}\right]' = 0, \quad [\beta_i]' = \left[\frac{h_{i+1}^2}{h_{i+1}^2 + h_i^2}\right]' = 0,$$

and $\mathbf{R}_i'(s_i, h_i) = \mathbf{T}_i(s_i)$, that is, $[\mathbf{R}_i(s_i, h_i)L_i^*(s_i, h_i)]' = \mathbf{T}_i(s_i)$. Then, we can get

$$\sum_{i=1}^{n} [\mathbf{R}_i(s_i, h_i)L_i^*(s_i, h_i)]' = \mathbf{T}_i(s_i). \tag{3.4}$$

Combine (3.3) and (3.4), we can obtain the result $(\mathbf{S}^{d,\mathbf{P}}(u, v))' = \mathbf{T}_i(s_i)$.

To sum up, the hybrid patch interpolate the cross-tangent function $\mathbf{T}_i(s_i)$ at the boundary. The proof is complete. □

We present an example of surface blending to illustrate the property of boundary derivative interpolation of the hybrid patch.

Example 3.2. Fig. 3.2(a) shows a five-sided hole composed of classical tensor-product B-spline patches, where each side of the hole is the B-spline curve with the same degree and knot vector. Given $d = 5, l = 3, n = 5$, we consider the same pentagonal parametric domain Γ as in Example 2.1. The $\mathbf{P}_i(s_i)$ and $\mathbf{T}_i(s_i)$ of the ribbon $\mathbf{R}_i$ are defined in (2.12). Fig. 3.2(b) shows the pentagonal hybrid patch $\mathbf{S}^{5,2}$ filling the five-sided hole by Theorem 3.2, where the black curves indicate the boundary curves of the hybrid patch.

Similarly, Fig. 3.2(d) shows a six-sided hole, with the B-spline curves of different degrees as the boundaries. Given $d = 6, l = 3, n = 6$, we consider the same hexagonal parametric domain Γ as in Example 3.1. The $\mathbf{P}_i(s_i)$ and $\mathbf{T}_i(s_i)$ of the ribbon $\mathbf{R}_i$ are defined in (2.11). Fig. 3.2(e) shows the hexagonal hybrid patch filling the six-sided hole by Theorem 3.2. Finally, Figs. 3.2(c) and 3.2(f) display the overall surface and its corresponding control points, respectively.

The conclusions we have obtained regarding boundaries are highly significant for surface blending. The hybrid patch behaves as B-spline curves with the same control points and B-spline basis functions on the boundaries. This boundary property indicates that a hybrid patch can be C^0 connected to other surfaces with B-spline boundaries. The boundary derivative interpolation property theoretically guarantees the hybrid patch interpolates the given cross-tangent $\mathbf{T}_i(s_i)$ of the ribbon $\mathbf{R}_i(s_i, h_i)$ on each side.

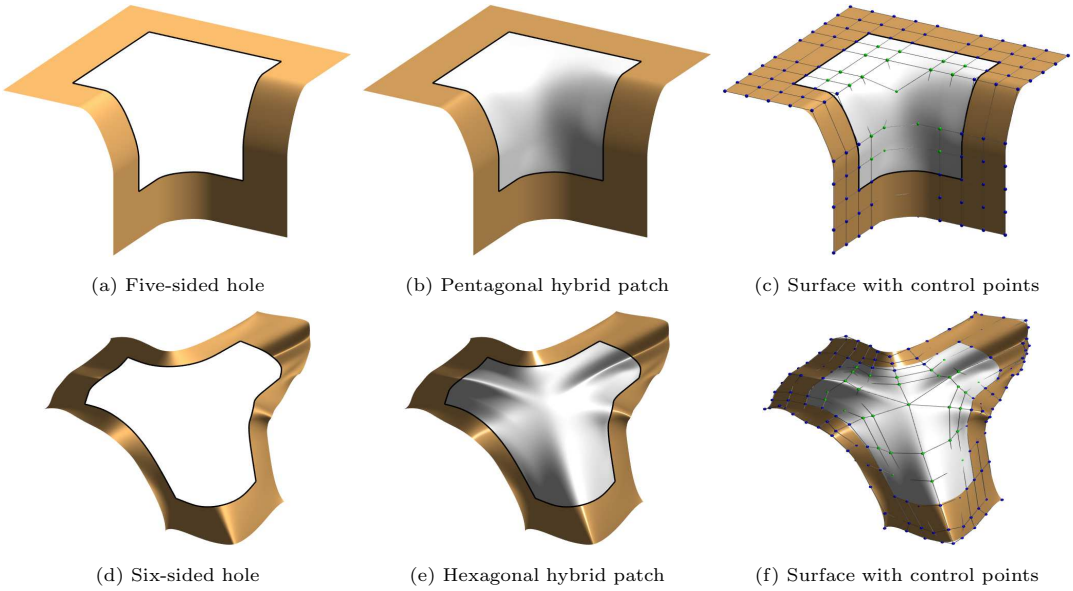

(a) Five-sided hole (b) Pentagonal hybrid patch (c) Surface with control points

(d) Six-sided hole (e) Hexagonal hybrid patch (f) Surface with control points

Fig. 3.2. Boundary derivative interpolation property of hybrid patches.

4. Improved Degree Elevation and Knot Insertion of Hybrid Patch

Degree elevation proposed in [18] can be used for increasing control points in the interior of the hybrid patch, but this changes the shape of the surface slightly. The elevated surface is not the same as the initial surface, so the flaw that makes the original degree elevation unsuitable for some applications, especially for IGA.

In this section, we focus on the geometric algorithms of the hybrid patch characterized by B-spline boundaries. We propose an improved degree elevation that keeps the surfaces and

boundaries unchanged while increasing the degree of the hybrid patch. In practical applications, surfaces with locality are more advantageous. Then we also propose a new knot insertion algorithm for the hybrid patch. In this study, we primarily focus on the hybrid patch characterized by B-spline boundaries of identical degree and knot vector, that is, the hybrid patch $\mathbf{S}^{d,p}(u,v)$ defined by (2.12). This choice is motivated by the patch's comprehensive properties and the simplicity of its mathematical representation. Although the hybrid patch $\mathbf{S}^{d,\mathbf{P}}(u,v)$ defined by Eq. (2.11) exhibits varying degrees and knot vectors for the B-splines on each boundary, the uniformity in the number of control vertices across all boundaries allows for the derivation of analogous conclusions.

4.1. Improved degree elevation

Our improved degree elevation is based on the iterative property of tensor-product Bernstein basis functions, that is

$$\begin{aligned} B_{j,k}^{d,d} = B_j^d B_k^d = \eta_{j+1}\upsilon_{k+1}B_{j+1,k+1}^{d+1,d+1} + (1-\eta_j)\upsilon_{k+1}B_{j,k+1}^{d+1,d+1} \\ + \eta_{j+1}(1-\upsilon_k)B_{j+1,k}^{d+1,d+1} + (1-\eta_j)(1-\upsilon_k)B_{j,k}^{d+1,d+1}, \end{aligned} \tag{4.1}$$

where

$$\eta_j = \frac{j}{d+1}, \quad \upsilon_k = \frac{k}{d+1}, \quad j = 0,\dots,d, \quad k = 2,\dots,l-1.$$

Denote the B-spline basis function $N_j^{p,\mathbf{U}^b}(s_i)$ of degree p by knot vector

$$\mathbf{U}^b = \{u_0,u_1,\cdots,u_{d+p+1}\} = \{\underbrace{t_0,\cdots,t_0}_{r_0-times},\underbrace{t_1,\cdots,t_1}_{r_1-times},\cdots,\underbrace{t_h,\cdots,t_h}_{r_h-times}\},$$

where $h+1$ represents the number of mutually different knots in $\mathbf{U}^b$, and r_i represents the multiplicity of knot $t_i (i=0,\dots,h)$ respectively. Then, we denote the knot vector after increasing the degree of the B-spline basis function by

$$\bar{\mathbf{U}}^b = \{\bar{u}_0,\bar{u}_1,\cdots,\bar{u}_{d+h+p+2}\} = \{\ \underbrace{t_0,\cdots,t_0}_{(r_0+1)-times}\ ,\ \underbrace{t_1,\cdots,t_1}_{(r_1+1)-times}\ ,\cdots,\ \underbrace{t_h,\cdots,t_h}_{(r_h+1)-times}\ \}. \tag{4.2}$$

The degree elevation of B-splines can be obtained using the Cohen-Lyche-Schumaker method [1]. Besides, we treat each $\mu_{j,k}^i \mathbf{C}_{j,k}^{d,i}$ in form as a new control point $\tilde{\mathbf{C}}_{j,k}^{d,i}$ of the hybrid patch. Then we obtain the following result.

Theorem 4.1. *Assume that*

$$\mathbf{U}^b = \{\underbrace{t_0,\cdots,t_0}_{r_0-times},\underbrace{t_1,\cdots,t_1}_{r_1-times},\cdots,\underbrace{t_h,\cdots,t_h}_{r_h-times}\},$$

then the hybrid patch is defined as

$$\mathbf{S}^{d,p}(u,v) = \sum_{i=1}^{n}\left[\sum_{j=0}^{d}\sum_{k=2}^{l-1}\tilde{\mathbf{C}}_{j,k}^{d,i}B_{j,k}^{d,d}(s_i,h_i) + \mathbf{R}_i(s_i,h_i)L_i^*(u,v)\right] + \mathbf{C}_0^d B_0^d(u,v), \tag{4.3a}$$

$$\mathbf{R}_i(s_i,h_i) = \mathbf{P}_i(s_i) + h_i\mathbf{T}_i(s_i) = \sum_{j=0}^{d}\mathbf{C}_{j,0}^{d,i}N_j^{p,\mathbf{U}^b}(s_i) + h_i\left(\sum_{j=0}^{d}\bar{\mathbf{C}}_{j,0}^{d,i}N_j^{p,\mathbf{U}^b}(s_i)\right), \tag{4.3b}$$

where

$$\tilde{\mathbf{C}}_{j,k}^{d,i} = \mu_{j,k}^{i}\mathbf{C}_{j,k}^{d,i}, \quad \bar{\mathbf{C}}_{j,0}^{d,i} = \frac{p}{\mathbf{U}_{p+j}^{b} - \mathbf{U}_{j}^{b}}\big(\mathbf{C}_{j,1}^{d,i} - \mathbf{C}_{j,0}^{d,i}\big).$$

The hybrid patch after degree elevation can be represented as

$$\tilde{\mathbf{S}}^{d+h,p+1}(u,v) = \sum_{i=1}^{n}\Bigg[\sum_{j=0}^{d+h}\sum_{k=2}^{l+h-1}\tilde{\mathbf{Q}}_{j,k}^{d+h,i}B_{j,k}^{d+h,d+h}(s_i,h_i) + \tilde{\mathbf{R}}_i(s_i,h_i)L_i^*(u,v)\Bigg] + \mathbf{C}_0^d B_0^d(u,v), \tag{4.4a}$$

$$\begin{aligned}\tilde{\mathbf{R}}_i(s_i,h_i) &= \mathbf{P}_i(s_i) + h_i\mathbf{T}_i(s_i)\\ &= \sum_{j=0}^{d+h}\mathbf{Q}_{j,0}^{d+h,i}N_j^{p+1,\bar{\mathbf{U}}^b}(s_i) + h_i\Bigg(\sum_{j=0}^{d+h}\bar{\mathbf{Q}}_{j,0}^{d+h,i}N_j^{p+1,\bar{\mathbf{U}}^b}(s_i)\Bigg),\end{aligned} \tag{4.4b}$$

where the B-spline basis functions $N_j^{p+1,\bar{\mathbf{U}}^b}$ *are defined by knot vector* $\bar{\mathbf{U}}^b$ *in* (4.2). *The control points* $\tilde{\mathbf{Q}}_{j,k}^{d+1,i}$ *satisfy*

$$\begin{aligned}\tilde{\mathbf{Q}}_{j,k}^{d+1,i} &= \eta_j\upsilon_k\tilde{\mathbf{C}}_{j-1,k-1}^{d,i} + (1-\eta_j)\upsilon_k\tilde{\mathbf{C}}_{j,k-1}^{d,i}\\ &\quad + \eta_j(1-\upsilon_k)\tilde{\mathbf{C}}_{j-1,k}^{d,i} + (1-\eta_j)(1-\upsilon_k)\tilde{\mathbf{C}}_{j,k}^{d,i},\end{aligned} \tag{4.5}$$

in which

$$\eta_j = \frac{j}{d+1}, \quad \upsilon_k = \frac{k}{d+1}, \quad j = 0,\ldots,d+1, \quad k = 2,\ldots,l.$$

Besides, for $j \notin \{0,\ldots,d\}$ *or* $k \notin \{2,\ldots,l-1\}$, *we set* $\tilde{\mathbf{C}}_{j,k}^{d,i} = \mathbf{0}$. *And the control points* $\mathbf{Q}_{j,0}^{d+h,i}$ *and* $\bar{\mathbf{Q}}_{j,0}^{d+h,i}$ *satisfy*

$$\mathbf{Q}_{j,0}^{d+h,i} = \frac{1}{p+1}\sum_{s=0}^{d}\mathbf{C}_{s,0}^{d,i}\Lambda_s^p(j), \quad \bar{\mathbf{Q}}_{j,0}^{d+h,i} = \frac{1}{p+1}\sum_{s=0}^{d}\bar{\mathbf{C}}_{s,0}^{d,i}\Lambda_s^p(j), \quad j = 0,\ldots,d+h, \tag{4.6}$$

where

$$\begin{aligned}\Lambda_s^p(j) &= \frac{\bar{u}_{j+p+1} - u_s}{u_{s+p} - u_s}\Lambda_s^{p-1}(j) + \frac{u_{s+p+1} - \bar{u}_{j+p+1}}{u_{s+p+1} - u_{s+1}}\Lambda_{s+1}^{p-1}(j) + \alpha_s^p(j),\\ \alpha_s^p(j) &= \frac{\bar{u}_{j+p} - u_s}{u_{s+p} - u_s}\alpha_s^{p-1}(j) + \frac{u_{s+p+1} - \bar{u}_{j+p}}{u_{s+p+1} - u_{s+1}}\alpha_{s+1}^{p-1}(j),\end{aligned}$$

starting with

$$\alpha_s^0(j) = \Lambda_s^0(j) = \begin{cases}1, & \bar{u}_j \in [u_i, u_{i+1}),\\ 0, & \textit{otherwise.}\end{cases}$$

Theorem 4.1 presents the degree elevation of the hybrid patch boundary from degree p to degree $p+1$ while keeps geometry and parameterization consistent. We compare the elevated hybrid patch with the original patch through the following example to show that our algorithm keeps the surface geometric invariant. To show the differences between the elevated surfaces and the original surfaces more clearly, we added texture mapping to the hybrid patch after degree elevation.

Example 4.1. Given $d = 6, l = 3$. The original B-spline basis functions in $\mathbf{R}_i$ are defined by the knot vector $\mathbf{U}^b = \{0, 0, 0, 0.2, 0.4, 0.6, 0.8, 1, 1, 1\}$ and degree $p = 2$. The initial pentagonal, hexagonal and octagonal hybrid patches are shown in Figs. 4.1(a)-4.1(c). The initial patches elevates degrees from $S^{6,2}$ to $S^{21,5}$ by the improved degree elevation, the elevated patches are shown in Figs. 4.1(d)-4.1(f). The elevated patches obtained by the proposed degree elevation in Theorem 4.1 remain geometry consistent with the original hybrid patches.

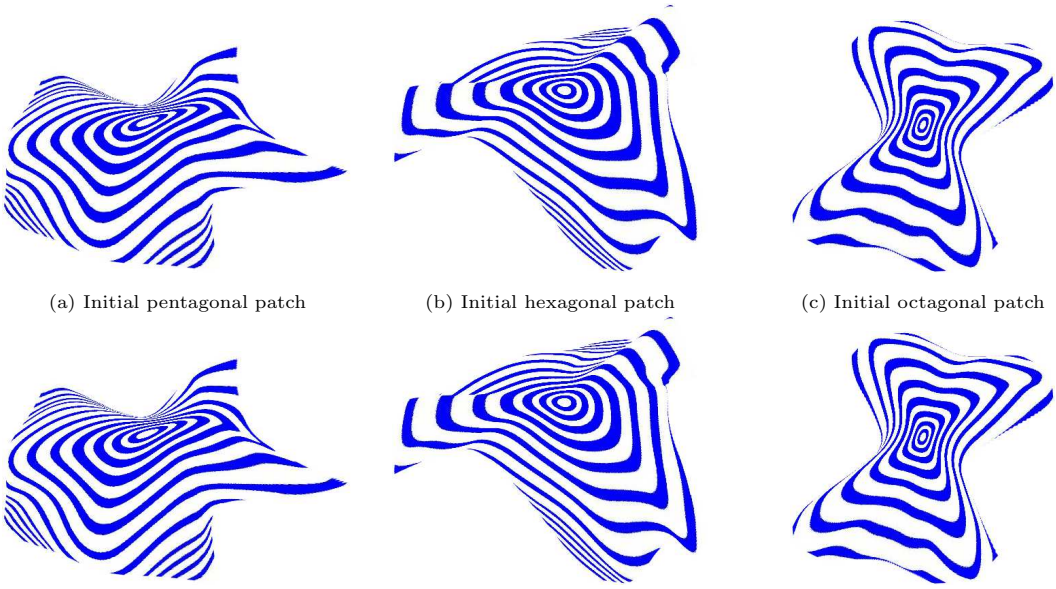

(a) Initial pentagonal patch (b) Initial hexagonal patch (c) Initial octagonal patch

(d) Resulting pentagonal hybrid patch after degree elevation (e) Resulting hexagonal hybrid patch after degree elevation (f) Resulting octagonal hybrid patch after degree elevation

Fig. 4.1. Comparison with the initial patches and the elevated results.

4.2. Knot insertion

We propose an knot insertion algorithm for hybrid patch in this section.The basic idea is that we deem a tensor-product Bernstein basis function $B_{j,k}^{d,d}$ of bi-degree d as a tensor product B-spline basis $N_{j,k}^{d,d}$ of the same degree over knot vectors

$$\mathbf{U} = \{\xi_1, \cdots, \xi_{2d+2}\} = \{ \underbrace{0, \cdots, 0}_{(d+1)-times} , \underbrace{1, \cdots, 1}_{(d+1)-times} \}$$

in the u-direction, and

$$\mathbf{V} = \{\eta_1, \cdots, \eta_{2d+2}\} = \{ \underbrace{0, \cdots, 0}_{(d+1)-times} , \underbrace{1, \cdots, 1}_{(d+1)-times} \}$$

in the v-direction. Thus, the original hybrid surface (2.4) is expressed as

$$\mathbf{S}^{d,p}(u, v) = \sum_{i=1}^{n} \left[\sum_{j=0}^{d} \sum_{k=2}^{l-1} \tilde{\mathbf{C}}_{j,k}^{d,i} N_{j,k}^{d,d}(s_i, h_i) + \mathbf{R}_i(s_i, h_i) L_i^*(u, v) \right] + \mathbf{C}_0^d B_0^d(u, v), \tag{4.7}$$

where $\mathbf{R}_i(s_i, h_i)$ is defined by (4.3b). We denote the spline spaces $\mathcal{S}^{d,d}_{\mathbf{U},\mathbf{V}}$ spanned by these tensor-product B-spline basis functions $N^{d,d}_{j,k}$, i.e. $\mathcal{S}^{d,d}_{\mathbf{U},\mathbf{V}} = \mathrm{span}(N^{d,d}_{j,k})$.

Denote the knot vector in the u-direction after inserting one new knot by

$$\bar{\mathbf{U}} = \{\bar{\xi}_1 = \xi_1, \bar{\xi}_2, \cdots, \bar{\xi}_{2d+3} = \xi_{2d+2}\} \supset \mathbf{U}.$$

And denote the knot vector in the v-direction after inserting one new knot by

$$\bar{\mathbf{V}} = \{\bar{\eta}_1 = \eta_1, \bar{\eta}_2, \cdots, \bar{\eta}_{2d+3} = \eta_{2d+2}\} \supset \mathbf{V}.$$

Then we have $\mathcal{S}^{d,d}_{\mathbf{U},\mathbf{V}} \subset \mathcal{S}^{d,d}_{\bar{\mathbf{U}},\bar{\mathbf{V}}}$ and the B-spline basis $\bar{N}^{d,d}_{j,k} \in \mathcal{S}^{d,d}_{\bar{\mathbf{U}},\bar{\mathbf{V}}}$.

Denote the knot vector of the B-spline basis function $N^{p,\mathbf{U}^b}_j(s_i)$ in $\mathbf{R}_i$ by

$$\mathbf{U}^b = \{u_0, u_1, \cdots, u_{d+p+1}\}.$$

And denote the knot vector after inserting one knot by

$$\bar{\mathbf{U}}^b = \{\bar{u}_0 = u_0, \bar{u}_1, \cdots, \bar{u}_{d+p+2} = u_{d+p+1}\}.$$

According to the knot insertion property of the B-spline basis functions, the relationship between the B-spline basis function N^d_j of degree d on the original knot vector and the B-spline basis function $\bar{N}^d_j$ on the new knot vector is as follows:

$$N^d_j = \alpha_j \bar{N}^d_j + \beta_j \bar{N}^d_{j+1}, \tag{4.8}$$

where

$$\alpha_j = \begin{cases} 1, & j = 0, \ldots, m-d, \\ \dfrac{\xi^* - \xi_j}{\xi_{j+d} - \xi_j}, & j = m-d+1, \ldots, m, \\ 0, & j = m+1, \ldots, d, \end{cases}$$

$$\beta_j = \begin{cases} 0, & j = 0, \ldots, m-d-1, \\ \dfrac{\xi_{j+d+1} - \xi^*}{\xi_{j+d+1} - \xi_{j+1}}, & j = m-d, \ldots, m-1, \\ 1, & j = m, \ldots, d, \end{cases}$$

and N^d_k and $N^{p,\mathbf{U}^b}_j$ are calculated in the same way. Then the $N^{d,d}_{j,k}$ in (4.7) can be calculated as

$$N^{d,d}_{j,k} = N^d_j N^d_k = \big(\alpha_j \bar{N}^d_j + \beta_j \bar{N}^d_{j+1}\big)\big(\alpha_k \bar{N}^d_k + \beta_k \bar{N}^d_{k+1}\big).$$

Finally, we conclude the following knot insertion algorithm of the hybrid patch as below result.

Theorem 4.2. *Assume that* $\{\underbrace{0, \cdots, 0}_{(d+1)-times}, \underbrace{1, \cdots, 1}_{(d+1)-times}\} \subset \bar{\mathbf{U}}, \{\underbrace{0, \cdots, 0}_{(d+1)-times}, \underbrace{1, \cdots, 1}_{(d+1)-times}\} \subset \bar{\mathbf{V}}$ *and* $\mathbf{U}^b = \{u_0, u_1, \cdots, u_{d+p+1}\}$*, then the hybrid patch in* (4.7) *can be represented as the following hybrid patch:*

$$\bar{\mathbf{S}}^{d,p}(u,v) = \sum_{i=1}^{n} \left[\sum_{j=0}^{d+1} \sum_{k=2}^{l} \tilde{\mathbf{Q}}^{d,i}_{j,k} \bar{N}^{d,d}_{j,k}(s_i, h_i) + \bar{\mathbf{R}}_i(s_i, h_i) L^*_i(u,v) \right] + \mathbf{C}^d_0 B^d_0(u,v), \tag{4.9a}$$

$$\bar{\mathbf{R}}_i = \mathbf{P}_i(s_i) + h_i \mathbf{T}_i(s_i) = \sum_{j=0}^{d+1} \mathbf{Q}^{d,i}_{j,0} \bar{N}^{p,\bar{\mathbf{U}}^b}_j(s_i) + h_i \left(\sum_{j=0}^{d+1} \bar{\mathbf{Q}}^{d,i}_{j,0} \bar{N}^{p,\bar{\mathbf{U}}^b}_j(s_i) \right), \tag{4.9b}$$

where $\bar{N}_{j,k}^{d,d}$ *are B-spline basis functions of spline space* $\mathcal{S}_{\bar{\mathbf{U}},\bar{\mathbf{V}}}^{d,d}$ *and* $\bar{N}_j^{p,\bar{\mathbf{U}}^b}$ *are defined by knot vector* $\bar{\mathbf{U}}^b$*. The control points* $\tilde{\mathbf{Q}}_{j,k}^{d,i}$, $\mathbf{Q}_{j,0}^{d,i}$ *and* $\bar{\mathbf{Q}}_{j,0}^{d,i}$ *satisfy*

$$\tilde{\mathbf{Q}}_{j,k}^{d,i} = \alpha_j\alpha_k\tilde{\mathbf{C}}_{j,k}^{d,i} + \alpha_j\beta_{k-1}\tilde{\mathbf{C}}_{j,k-1}^{d,i} + \beta_{j-1}\alpha_k\tilde{\mathbf{C}}_{j-1,k}^{d,i} + \beta_{j-1}\beta_{k-1}\tilde{\mathbf{C}}_{j-1,k-1}^{d,i}, \tag{4.10}$$

$$\mathbf{Q}_{j,0}^{d,i} = \alpha_j\mathbf{C}_{j,0}^{d,i} + \beta_{j-1}\mathbf{C}_{j-1,0}^{d,i}, \tag{4.11}$$

$$\bar{\mathbf{Q}}_{j,0}^{d,i} = \alpha_j\bar{\mathbf{C}}_{j,0}^{d,i} + \beta_{j-1}\bar{\mathbf{C}}_{j-1,0}^{d,i}. \tag{4.12}$$

Besides, for $j \notin \{0,\ldots,d\}$ *or* $k \notin \{2,\ldots,l-1\}$*, we set* $\tilde{\mathbf{C}}_{j,k}^{d,i} = \mathbf{0}$.

Theorem 4.2 presents the knot insertion of the hybrid patch which keeps geometry consistent. We compare the refined surface with the original surface through the following example to show that our knot insertion algorithm keeps the consistency of the surface.

Example 4.2. Given $d = 6, l = 3, p = 2$. The original knot vectors of the hybrid patches are defined as

$$\mathbf{U} = \mathbf{V} = \{\underbrace{0,\cdots,0}_{(d+1)-times}, \underbrace{1,\cdots,1}_{(d+1)-times}\}, \quad \mathbf{U}^b = \{0,0,0,0.2,0.4,0.6,0.8,1,1,1\}. \tag{4.13}$$

The initial pentagonal, hexagonal and octagonal hybrid patches are shown in Figs. 4.2(a)-4.2(c). Then, we insert 5 new knots into the knot vectors $\mathbf{U}$, $\mathbf{V}$ and $\mathbf{U}^b$ of the initial hybrid patches respectively. The refined patches using the knot insertion algorithm proposed in Theorem 4.2 are shown in Figs. 4.2(d)-4.2(f). We remark that the resulting patches obtained by our algorithm keep hybrid patches consistently.

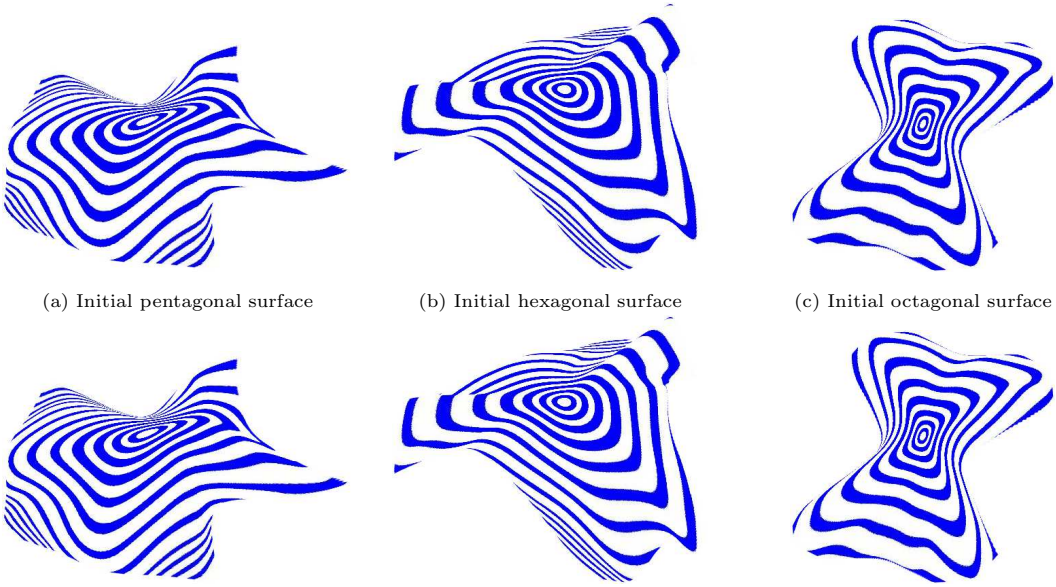

(a) Initial pentagonal surface (b) Initial hexagonal surface (c) Initial octagonal surface

(d) Resulting pentagonal hybrid patch after knot insertion (e) Resulting hexagonal hybrid patch after knot insertion (f) Resulting octagonal hybrid patch after knot insertion

Fig. 4.2. Comparison with the initial patches and the refined results.

Remark 4.1. In the proposed methods, we keep $\mathbf{C}_0^d$ and its corresponding basis function and the weight sum of the two rows L_i^* the same as the initial hybrid patch $\mathbf{S}^{d,p}$. This treatment is the key point to keep the elevated/refined surface unchanged and avoid redundant computation.

5. Conclusions and Future Work

In this paper, we focus on the geometric properties and algorithms of the hybrid patch with B-spline boundaries based on the multi-sided surface scheme proposed in [18]. We present the boundary interpolation and boundary derivative interpolation of the hybrid patch. We then propose an improved degree elevation algorithm and a new knot insertion algorithm of the hybrid patch. The degree elevation algorithm increases the degree of the surface to facilitate surface refinement while maintaining geometric consistency. Meanwhile, the knot insertion algorithm increases the DOFs by adding control points at specific locations, allowing for more precise adjustments to the surface shape.

The results we get regarding the boundary can be applied to surface blending and hole filling by polygonal surfaces, which will be our future work. In addition, our future research will focus on constructing the high-quality suitable-analysis parameterization in IGA by hybrid patch from complex multi-sided CAD models with given B-spline boundaries. The p, h and k refinements for analysis in IGA can be derived using the degree elevation and knot insertion algorithms proposed in this paper. Furthermore, we will consider to construct control point-based multi-sided solid with B-spline boundaries and study its geometric properties and algorithms in future.

Acknowledgements. The authors would like to thank Dr. Péter Salvi, Budapest University of Technology and Economics, Hungary, for valuable discussions of the hybrid patch.

This research was supported by the National Natural Science Foundation of China (Grant Nos. 12471358, 12071057).

References

[1] E. Cohen, T. Lyche, and L.L. Schumaker, Algorithms for degree-raising of splines, *ACM Trans. Graphics*, **4**:3 (1985), 171–181.

[2] J.A. Cottrell, T.J.R. Hughes, and Y. Bazilevs, *Isogeometric Analysis: Toward Integration of CAD and FEA*, Wiley Publishing, 2009.

[3] J.A. Cottrell, A. Reali, Y. Bazilevs, and T.J.R. Hughes, Isogeometric analysis of structural vibrations, *Comput. Methods Appl. Mech. Engrg.*, **195**:41-43 (2006), 5257–5296.

[4] G. Farin, *Curves and Surfaces for CAGD: A Practical Guide*, Morgan Kaufmann, 2002.

[5] M.S. Floater, Wachspress and mean value coordinates, in: *Approximation Theory XIV: San Antonio* 2013. *Springer Proceedings in Mathematics & Statistics*, Springer, (2014), 81–102.

[6] L. García-Puente, F. Sottile, and C.G. Zhu, Toric degenerations of Bézier patches, *ACM Trans. Graphics*, **30**:5 (2011), 110.

[7] R. Goldman, *Pyramid Algorithm: A Dynamic Programming Approach to Curves and Surfaces for Geometric Modeling*, Morgan Kaufmann, 2003.

[8] R. Goldman, Multisided arrays of control points for multisided Bézier patches, *Comput. Aided Geom. Des.*, **21**:3 (2004), 243–261.

[9] T.J.R. Hughes, J.A. Cottrell, and Y. Bazilevs, Isogeometric analysis: CAD, finite elements, NURBS, exact geometry and mesh refinement, *Comput. Methods Appl. Mech. Engrg.*, **194**:39-41 (2005), 4135–4195.

[10] Y. Ji, J.G. Li, Y.Y. Yu, and C.G. Zhu, h-Refinement method for toric parameterization of planar multi-sided computational domain in isogeometric analysis, *Comput. Aided Geom. Des.*, **93** (2022), 102065.

[11] K. Karčiauskas and J. Peters, Improved caps for improved subdivision surfaces, *Comput.-Aided Des.*, **162** (2023), 103543.

[12] R. Krasauskas, Toric surface patches, *Adv. Comput. Math.*, **17** (2002), 89–113.

[13] J.G. Li, Y. Ji, and C.G. Zhu, De Casteljau algorithm and degree elevation of toric surface patches, *J. Syst. Sci. Complex.*, **34** (2021), 21–46.

[14] C.T. Loop and T.D. Derose, A multisided generalization of Bézier surfaces, *ACM Trans. Graphics*, **8**:3 (1989), 204–234.

[15] S. Mann, Investigations of a functional version of a blending surface scheme for regular data interpolation, *Comput. Aided Geom. Des.*, **111** (2024), 102345.

[16] L. Piegl and W. Tiller, *The NURBS Book*, Springer Science & Business Media, 1997.

[17] K.K. Qin, J. Li, and C.Y. Deng, Blending Bézier patch for multi-sided surface modeling, *Comput. Aided Geom. Des.*, **105** (2023), 102222.

[18] P. Salvi, Intuitive interior control for multi-sided patches with arbitrary boundaries, *Comput.-Aided Des. Applic.*, **21**:1 (2024), 143–154.

[19] P. Salvi and T. Várady, Multi-sided Bézier surfaces over concave polygonal domains, *Comput. Graphics*, **74** (2018), 56–65.

[20] P. Salvi, T. Várady, and A. Rockwood, Ribbon-based transfinite surfaces, *Comput. Aided Geom. Des.*, **31**:9 (2014), 613–630.

[21] L.Y. Sun and C.G. Zhu, G^1 continuity between toric surface patches, *Comput. Aided Geom. Des.*, **35–36** (2015), 255–267.

[22] L.Y. Sun and C.G. Zhu, Curvature continuity conditions between adjacent toric surface patches, *Comput. Graph. Forum*, **37**:7 (2018), 469–477.

[23] M. Vaitkus, T. Várady, P. Salvi, and Á. Sipos, Multi-sided B-spline surfaces over curved, multi-connected domains, *Comput. Aided Geom. Des.*, **89** (2021), 102019.

[24] T. Várady, A. Rockwood, and P. Salvi, Transfinite surface interpolation over irregular n-sided domains, *Computer-Aided Des.*, **43**:11 (2011), 1330–1340.

[25] T. Várady, P. Salvi, and G. Karikó, A multi-sided Bézier patch with a simple control structure, *Comput. Graph. Forum*, **35**:2 (2016), 307–317.

[26] T. Várady, P. Salvi, and I. Kovács, Enhancement of a multi-sided Bézier surface representation, *Comput. Aided Geom. Des.*, **55** (2017), 69–83.

[27] T. Várady, P. Salvi, and A. Rockwood, Transfinite surface interpolation with interior control, *Graph. Models*, **74** (2012), 311–320.

[28] T. Várady, P. Salvi, and M. Vaitkus, Generalized Bézier and B-spline patches with exact refinement, in: *Proceedings of the Eleventh Hungarian Conference on Computer Graphics and Geometry*, ACM, (2024), 58–62.

[29] T. Várady, P. Salvi, M. Vaitkus, and Á. Sipos, Multi-sided Bézier surfaces over curved, multi-connected domains, *Comput. Aided Geom. Des.*, **78** (2020), 101828.

[30] M.Y. Wang, Y. Ji, and C.G. Zhu, Degree elevation and knot insertion for generalized Bézier surfaces and their application to isogeometric analysis, *J. Comput. Math.*, **42**:5 (2024), 1197–1225.

[31] G. Xu et al., Constructing IGA-suitable planar parameterization from complex CAD boundary by domain partition and global/local optimization, *Comput. Methods Appl. Mech. Engrg.*, **328** (2018), 175–200.

[32] Y.Y. Yu, Y. Ji, and C.G. Zhu, An improved algorithm for checking the injectivity of 2D toric surface patches, *Comput. Math. Appl.*, **79** (2020), 2973–2986.

[33] X.F. Zhu, Y. Ji, C.G. Zhu, P. Hu, and Z.D. Ma, Isogeometric analysis for trimmed CAD surfaces using multi-sided toric surface patches, *Comput. Aided Geom. Des.*, **79** (2020), 101847.